J. Fluid Mech. (2002), *vol.* 473, *pp.* 83–101.
DOI: 10.1017/S0022112002002276 Printed in the United Kingdom

Numerical simulation of the wake of a towed sphere in a weakly stratified fluid

By DOUGLAS G. DOMMERMUTH[1], JAMES W. ROTTMAN[1], GEORGE E. INNIS[1] AND EVGENY A. NOVIKOV[2]

[1]Naval Hydrodynamics Division, Science Applications International Corporation, 10260 Campus Point Drive, MS C4, San Diego, CA 92121-1578, USA

[2]Institute of Nonlinear Science, University of California, San Diego, 9500 Gilman Drive, La Jolla, CA 92093-0402, USA

(Received 20 December 2000 and in revised form 28 June 2002)

We present some preliminary results from using large-eddy simulation to compute the late wake of a sphere towed at constant speed through a non-stratified and a uniformly stratified fluid. The wake is computed in each case for two values of the Reynolds number: $Re = 10^4$, which is comparable to that used in laboratory experiments, and $Re = 10^5$. An important aspect of the simulation is the use of an iterative procedure to relax the initial turbulence field so that the normal and shear turbulent stresses are properly correlated and the turbulent production and dissipation are in equilibrium. For the lower Reynolds number our results compare well with existing laboratory experimental results. For the higher Reynolds number we find that even though the turbulence is more developed and the wake contains finer structure, most of the similarity properties of the wake are unchanged compared with those observed at the lower Reynolds number.

1. Introduction

Laboratory experiments on the evolution of the turbulent wake generated by a body towed through a stratified fluid have shown that, if the stratification is not too strong, the evolution of the wake can be divided into three phases: a near-wake phase, a transition phase and a far-wake phase. In the near-wake phase the wake spreads uniformly in all three dimensions and the turbulence behaves as it does for a similar wake in a homogeneous fluid. At some point downstream the wake has expanded sufficiently far vertically so that buoyancy effects become important and the wake begins to collapse vertically as it continues to spread horizontally. This is the beginning of the transition phase in which much of the turbulent kinetic energy that has been converted to potential energy in the near wake is converted back to kinetic energy. Finally, further downstream, the vertical motion in the wake diminishes to nearly zero. This is the beginning of the far-wake phase, which is characterized by horizontally large and vertically relatively thin eddy-like dipole structures, often referred to by the descriptive name of 'pancake eddies', that persist for very long distances downstream.

The near-wake phase has been well-studied in the laboratory for a sphere towed through a uniformly stratified fluid, for $Re \leqslant 10^4$ and $Fr \leqslant 20$, where the Reynolds number $Re = UD/\nu$ and the Froude number $Fr = U/ND$, in which U is the tow

speed, D is the diameter of the sphere and N is the buoyancy frequency. The studies of Lin *et al.* (1992*b*), Lin, Boyer & Fernando (1992*a*, 1994), Chomaz *et al.* (1992) and Chomaz, Bonneton & Hopfinger (1993*b*) show that the turbulence properties of the near wake are highly dependent on the values of Re and Fr.

At the beginning of the transition phase the vertical growth of the wake stops and the decay rates of the turbulence quantities abruptly change. This wake collapse period was first defined by Schooley & Stewart (1963), and is discussed in greater detail in Lin *et al.* (1992*b*), Spedding, Browand & Fincham (1996*a*, *b*), Spedding (1997), Bonnier, Eiff & Bonneton (2000) and Spedding (2001). Spedding (1997) refers to this period as an adjustment, or non-equilibrium (NEQ), period in which the conversion of potential energy to kinetic energy reduces the decay rates of the turbulent kinetic energy.

The final, or far-wake, phase of the wake evolution is characterized by very persistent slowly evolving thin eddy dipole structures. Early, primarily qualitative, studies of these far-wake features are reported by Pao & Kao (1977), Kao & Pao (1978) and Lin & Pao (1979). More extensive visualization studies are reported by Hopfinger (1987), Sysoeva & Chashechkin (1991) and Chomaz *et al.* (1993*a*, *b*). Quantitative studies of the vorticity structure of the far wake are reported in Spedding *et al.* (1996*a*, *b*) and Spedding (1997, 2001). The vertical velocity and density structure of these late-wake vortices is investigated by Bonnier, Bonneton & Eiff (1998), Bonnier *et al.* (2000) and Spedding (2002). Based on their experimental results, Bonnier *et al.* (1998, 2000) propose a three-dimensional model for the quasi-equilibrium structures that exist in the far wake. Numerical studies of the far wake in a stratified fluid include the Reynolds-averaged hydrostatic simulations using a simple Smagorinsky turbulence closure model described in Fung & Chang (1996) and the direct numerical simulations (DNS) reported in Gourlay *et al.* (2001). A review of the main features of the late stratified wake is given by Riley & Lelong (2000).

At large Re and Fr, the precise nature of the mechanism responsible for the formation of the far-wake eddies is still not understood. It has been speculated, Pao & Kao (1977), that these could be due to the helical vortex shed by the sphere that persist into the far wake. Spedding (2001) concludes from his experimental results that a combination of the Kelvin–Helmholtz instability and spiral mode instabilities can account for the observed wavelengths in the late wake. On the other hand, the experiments of Bonnier *et al.* (1998), among others, show that the late-wake eddies appear whether a helical vortex exists in the near wake or not, so it seems that a helical vortex is not *required* for their existence. Also, the numerical simulations of Dommermuth *et al.* (2000) and Gourlay *et al.* (2001) indicate that even completely incoherent turbulence in the near wake with no imbedded features at all still gives rise to late-wake eddy structure. The other major theory of the mechanism responsible for the formation of the late-wake eddies is that they develop from some instability of the mean wake flow that is reinforced by the stable stratification. This idea is favoured by Fung & Chang (1996), although their calculations can be interpreted as indicating that the late-wake eddies are produced by coherent structures introduced through the initial conditions.

In this paper we develop a numerical procedure intended for the simulation of the far wake and the transition to the far wake. In particular we are interested in how the late wakes are affected if the Reynolds number is much higher than has been obtained in the laboratory studies. We report four numerical experiments: the first is an attempt to simulate the formation of eddies in the late wake due to a turbulent flow for the stratified case with $Fr = 2$, the smallest value of Fr for which

there is a transition phase, and $Re = 10^4$, the largest value of Re for which laboratory experiments have been performed. The second is similar to the first except that the fluid is non-stratified ($Fr = \infty$). The last two numerical experiments are similar to the first two, except the Reynolds number is higher ($Re = 10^5$). This latter value of Re is higher than has been obtained so far in laboratory experiments.

The numerical method is large-eddy simulation (LES). Our interest is in resolving the large-scale turbulent eddies so that we can gain insight into how these develop into the large-scale, quasi-two-dimensional vortex structures that are observed in the far wake. Also, we are interested in how individual eddies interact with the background stratification to generate the random internal waves first observed in the experiments of Gilreath & Brandt (1985). A Reynolds-averaged model, such as that used by Fung & Chang (1996) or the EDQNM model used by Staquet & Godeferd (1998) may be adequate for the late wake but will not provide the detailed eddy structure we seek in the intermediate wake regime. LES gives sufficient detail to provide insight into the mechanisms that lead to the end of the transition phase and that develop into the far-wake eddies, yet can still handle higher values of Re than has been achieved in the experiments. The flow is initialized with a mean deficit wake flow with a superimposed homogeneous turbulent flow field. A relaxation procedure is introduced to obtain the proper initial conditions for all the turbulence quantities before the calculation is begun. This relaxation procedure proved to be important, for without it the onset times of the different similarity phases of the wake were not properly simulated.

In this paper we focus on the velocity structure of the far wake. There is no coherent structure imposed on the turbulence other than the gross characteristics of the mean wake flow. Our results show that coherent vortices appear in the late wake even though the flow is initialized without any coherent structures. The results of these numerical simulations at the lower Re compare very well with the late-wake experimental results of towed spheres, even though only the mean flow characteristics are matched in the near field. For the higher Reynolds number we find that even though the turbulence is more developed and the wake contains finer structure, most of the similarity properties of the wake are unchanged compared with those observed at the lower Reynolds number.

2. Problem formulation

A schematic drawing of the flow under consideration is shown in figure 1 in a reference frame in which the sphere is at rest. This figure serves to define much of the nomenclature used here. The wake behind the sphere is considered to be statistically stationary. Since the entire wake is too long to compute as a whole, we make the approximation that the flow can be computed within a rectangular box, with axial dimensions much smaller than the total length of the wake, that moves with the mean flow speed U. Within this box the flow is computed using large-eddy simulation (LES).

2.1. *Large-eddy formulation of the Boussinesq equations*

We assume that the fluid is incompressible and in the undisturbed state is homogeneous in the horizontal and uniformly stratified in the vertical. A large-eddy approximation is invoked whereby the large-scale features of the flow are resolved and the small scales are modelled. Let u_i ($i = 1, 2, 3$) denote the three-dimensional velocity field as a function of space x_i and time t. The origin of the coordinate system is at the centroid of the sphere, as shown in figure 1; x_1 is positive upstream, x_2 is transverse

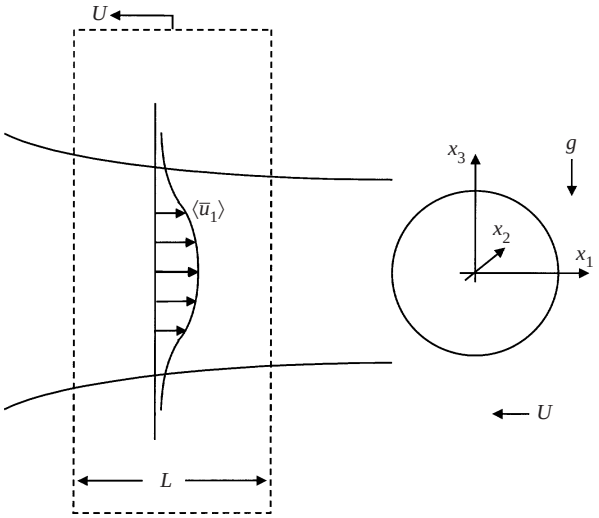

FIGURE 1. A schematic diagram of the sphere and the coordinate system in a reference frame in which the sphere is at rest. The dashed box denotes the slab of fluid that is modelled using LES. $\langle \bar{u}_1 \rangle$ is the wake deficit.

to the track of the sphere, and x_3 is positive upward. The length and velocity scales of the flow are respectively normalized by the diameter of the sphere, D, and the free-stream velocity, U. The governing non-dimensional parameters for this flow are the Reynolds number $Re = UD/\nu$, the Schmidt number $Sc = \nu/\kappa$ and the Froude number $Fr = U/(ND)$, where ν is the kinematic viscosity of the fluid, κ is the diffusivity of the scalar in the fluid that changes its density and $N = [(-g/\rho_o)\partial\varrho/\partial x_3]^{1/2}$ is the buoyancy (or Brunt–Väisälä) frequency in which g is the acceleration due to gravity, ρ_o is the mean density, and $\partial\varrho/\partial x_3$ is the vertical derivative of the background mean density (assumed to be a constant).

The large-scale features of the flow are determined by applying a spatial filter to the equations of motion. We used a top-hat (or box) filter with width equal to the grid spacing. The filtered equation of continuity is

$$\frac{\partial \bar{u}_i}{\partial x_i} = 0, \tag{2.1}$$

where the overbar denotes spatial filtering.

The density equation is

$$\frac{\partial \bar{\rho}}{\partial t} + \frac{\partial \bar{u}_j \bar{\rho}}{\partial x_j} - \bar{u}_3 = \frac{1}{Re\, Sc} \frac{\partial^2 \bar{\rho}}{\partial x_j \partial x_j} - \frac{\partial \theta_j}{\partial x_j}, \tag{2.2}$$

where $\bar{\rho}$ is the perturbation density, which is normalized by the incremental change in background density over the diameter of the sphere, $-D\partial\varrho/\partial x_3$. The residual flux of density is

$$\theta_j = \overline{u_j \rho} - \bar{u}_j \bar{\rho}. \tag{2.3}$$

The filtered momentum conservation equations for a weakly stratified fluid are

$$\frac{\partial \bar{u}_i}{\partial t} + \frac{\partial \bar{u}_j \bar{u}_i}{\partial x_j} = -\frac{\partial \bar{p}}{\partial x_i} + \frac{1}{Re} \frac{\partial}{\partial x_j} \left(2\mu \bar{S}_{ij}\right) - \delta_{i3} \frac{\bar{\rho}}{Fr^2} - \frac{\partial \tau_{ij}}{\partial x_j}, \tag{2.4}$$

where p is the dynamic pressure, which is normalized by $\rho_o U^2$, and $\mu(\rho)$ is a constitutive relation between the viscosity and the density of the fluid. Here, we assume $\mu(\rho) = 1$.

$\bar{S}_{ij}$ is the filtered strain tensor:

$$\bar{S}_{ij} = \frac{1}{2}\left(\frac{\partial \bar{u}_i}{\partial x_j} + \frac{\partial \bar{u}_j}{\partial x_i}\right). \tag{2.5}$$

τ_{ij} is the subgrid-scale (SGS) stress tensor:

$$\tau_{ij} = \overline{u_j u_i} - \bar{u}_j \bar{u}_i. \tag{2.6}$$

A mixed model (Bardina, Ferziger & Reynolds 1984) is used to model the SGS stress tensor. The mixed model was chosen as it is a first step towards implementing a dynamic SGS model, such as the one described by Germano *et al.* (1991). For the mixed model the SGS stress tensor is modelled as

$$\tau_{ij} = \left(\overline{\bar{u}_j \bar{u}_i} - \bar{\bar{u}}_j \bar{\bar{u}}_i\right) - c_s \Delta^2 |\bar{\mathscr{S}}| \bar{S}_{ij}, \tag{2.7}$$

The first term, in parentheses, on the right-hand side of (2.7) is the similarity portion of the mixed model. It provides an accurate representation of the turbulent stresses. The remaining term on the right-hand side is the Smagorinsky portion of the mixed model. It represents dissipation. Also, c_s is the Smagorinsky coefficient and Δ is the width of the spatial filter, which as mentioned earlier we set equal to the grid spacing. The magnitude of the strain tensor is defined

$$|\bar{\mathscr{S}}| = \sqrt{\bar{S}_{ij} \bar{S}_{ij}}. \tag{2.8}$$

The corresponding model for the residual density flux combines a similarity model with an eddy diffusivity model:

$$\theta_j = \left(\overline{\bar{u}_j \bar{\rho}} - \bar{\bar{u}}_j \bar{\bar{\rho}}\right) - c_\theta \Delta^2 |\bar{\mathscr{S}}| \frac{\partial \bar{\rho}}{\partial x_j}, \tag{2.9}$$

where c_θ is the eddy diffusivity constant. The values of the turbulence coefficients used herein are $c_s = c_\theta = 0.075$, which have been chosen such that the relaxation procedure described below gives the best approximation to the $Fr = \infty$ laboratory data at $x_1 = -6$. Studies completed since these calculations were performed indicate that these coefficients should be smaller. In the high Reynolds number ($Re = 10^5$) runs, the molecular viscosity term contributed only 6% of the momentum diffusion, with the SGS terms contributing the remaining 94%. In the low Reynolds number ($Re = 10^4$) runs, in which the turbulence is nearly resolved, the molecular viscosity term contributed nearly 40% of the momentum diffusion.

In this paper, the Schmidt number is assumed to be infinite. This is representative of fluids with large Schmidt numbers, such as salt water (for which $Sc \approx 700$) in the near and intermediate wake regimes. For such large Schmidt numbers the molecular diffusion term in (2.2) is always much smaller than the divergence of the residual density flux in the near and intermediate wake. Far enough downstream where the eddy scales become very large the finite value of the Schmidt number may be important, but in the calculations presented here we have neglected this effect.

2.2. *Galilean approximation*

Following Orszag & Pao (1974), a Galilean approximation is used to relate the spatial development of the wake to the temporal evolution of the LES. In normalized variables, let $x_1 = -t$, where x_1 is the distance downstream of the sphere in the wake

and t is the corresponding time in the LES. Based on this Galilean approximation, we further assume that

$$\widehat{\phi} = \frac{1}{T}\int_0^T \mathrm{d}t\phi(t, x = X_o) \Longleftrightarrow \frac{1}{L}\int_0^L \mathrm{d}x\phi(t = T_o, x) = \langle\phi\rangle, \tag{2.10}$$

where ϕ is a physical quantity, the hat denotes time averaging, angle brackets denote spatial averaging, L is the length of the LES computational domain in the axial direction (see figure 1), T is the duration of time averaging, and X_o and T_o are positions in space and time where the wake of the sphere and the LES correspond. A tilde denotes the turbulent fluctuations, which are defined as $\widetilde{\phi} = \phi - \langle\phi\rangle$. As shown in figure 1, the wake of the sphere is modelled as a slab of fluid.

2.3. *Initialization*

The initial velocity field is decomposed into a mean disturbance and a fluctuating disturbance. The magnitude and distribution of mean and fluctuating components are specified based on the measurements of Bevilaqua & Lykoudis (1978). For the mean flow along the track of the sphere

$$\langle\bar{u}_1\rangle = a_o \exp\left(-\frac{r^2}{2r_o^2}\right), \tag{2.11}$$

where a_o is the amplitude of the mean wake deficit normalized by the velocity, and r_o is the initial characteristic radius of the wake. The cross-stream components, $\langle\bar{u}_2\rangle$ and $\langle\bar{u}_3\rangle$, are initially set equal to zero. The initial r.m.s. velocity fluctuations are approximated using the function

$$\sqrt{\langle\tilde{\bar{u}}_i\tilde{\bar{u}}_i\rangle} = a_1\left(1 + \frac{r^2}{r_o^2}\right)\exp\left(-\frac{r^2}{2r_o^2}\right), \tag{2.12}$$

where a_1 is the initial amplitude of the r.m.s. velocity fluctuations. The fluctuating velocity field is constructed from a realization of fully developed homogeneous turbulence that is projected onto the r.m.s. velocity distribution, as is described in more detail in Dommermuth *et al.* (1997). The r.m.s. fluctuations are initially uncorrelated and the turbulent shear stresses are zero. As explained in § 3.1, an iterative procedure is used to relax the wake to produce accurate distributions of the turbulent shear stresses. We assume that the mean and fluctuating portions of the density disturbance are initially zero.

2.4. *Numerical algorithm*

Equations (2.1)–(2.9) are discretized using second-order finite differences. A fully staggered grid is used in the numerical simulations. Periodic boundary conditions are used along the sides of the computational domain, and free-slip boundary conditions are imposed at the top and bottom. A third-order Runge–Kutta scheme is used to integrate the equations with respect to time. The numerical algorithms have been implemented using high-performance Fortran (PGHPF) on a CRAY T3E. Additional details and convergence studies of a similar numerical algorithm are described in Dommermuth *et al.* (1997).

3. Results

The initial mean velocity disturbance and r.m.s. fluctuations are based on least-squares fits to the laboratory measurements of Bevilaqua & Lykoudis (1978). Their

experiments were for a towed sphere in a neutrally stratified fluid at a Reynolds number $Re = 10^4$. The fits to the data were made at the cross-section of the wake six diameters downstream of the sphere. For the mean flow, $a_o = 0.110$ and $r_o = 0.50$. For the fluctuating portion of the flow, $a_1 = 0.045$. Convergence is established using two different grid resolutions corresponding to coarse ($128 \times 256 \times 129$ grid points) and fine ($256 \times 512 \times 257$ grid points) simulations. For the coarse-grid simulations we chose a computational domain that is $24D$ long, $24D$ wide, and $12D$ deep. For the fine-grid simulations we chose a computational domain that is $12D$ long, $24D$ wide, and $12D$ deep. This coarse-grid domain is long enough in the axial direction to contain four pairs of pancake eddies, based on figure 3 of Spedding *et al.* (1996*a*), and the fine-grid domain contains two pairs of pancake eddies. The fine-grid results are presented here.

In order to investigate the effects of Reynolds number and stratification, simulations were performed at Reynolds numbers of $Re = 10^4$ and 10^5 for Froude numbers of $Fr = 2$ and ∞. The same mean-flow and r.m.s. fluctuating velocity profiles are imposed initially for all cases.

3.1. *Wake relaxation*

A relaxation procedure is used to produce the appropriate turbulent shear stress profiles at the beginning of the calculation. During the relaxation procedure, the mean and r.m.s. fluctuating velocity distributions of the flow are held fixed. The total turbulent kinetic energy is also held fixed, but the spatial distributions of the turbulent shear stresses are free to vary. Once the turbulent shear stresses have come to an equilibrium distribution, the relaxation procedure is turned off and the numerical simulation is initiated. A similar procedure is used by Orszag & Pao (1974) in their numerical simulations of a self-propelled body.

The dissipation rate ϵ_t of the turbulent kinetic energy is

$$\epsilon_t = \int_{\mathscr{V}} \bar{u}_i \frac{\partial \tilde{\tilde{u}}_j \tilde{\tilde{u}}_i}{\partial x_j} \, \mathrm{d}V + \int_{\mathscr{V}} \frac{\tilde{\tilde{u}}_3 \tilde{\tilde{\rho}}}{Fr^2} \, \mathrm{d}V + \int_{\mathscr{V}} \frac{\tilde{\tilde{u}}_i}{Re} \frac{\partial}{\partial x_j} \left(2\mu \tilde{\tilde{S}}_{ij} \right) \mathrm{d}V - \int_{\mathscr{V}} \tilde{\tilde{u}}_i \frac{\partial \tilde{\tau}_{ij}}{\partial x_j} \, \mathrm{d}V, \qquad (3.1)$$

where $\mathscr{V}$ is the volume of the fluid. The first integral is the production of turbulent kinetic energy, the second integral is the energy radiated by internal waves, the third integral is the energy dissipated due to viscous dissipation, and the fourth integral is the energy dissipation associated with SGS interactions. In well-developed turbulent flows, $\epsilon_t \approx 0$, and turbulent production balances turbulent dissipation.

The evolution of the turbulent production rate and the total dissipation rate during this relaxation procedure is shown in figure 2 for $Re = 10^4$ and 10^5 for neutral ($Fr = \infty$) stratification. The total dissipation rate is the sum of the last two integrals on the right-hand side of (3.1). Initially the turbulent production is zero and the total dissipation rate is too high. As time increases, the turbulent production increases and the dissipation rate decreases. The numerical simulation is initiated when turbulent production and dissipation become approximately constant with time, at $t \approx 30$ in both cases. With this procedure, turbulent shear stresses are properly determined at the beginning of the calculation. Note that turbulent production and dissipation are not in balance at this stage. Apparently, the turbulence in the wake is not self-similar this near to the sphere. If the wake simulation had been initialized with the data at $t = 0$ in figure 2, the turbulent fluctuations would have decayed too rapidly and the mean portion of the flow would have decayed too slowly because the turbulent dissipation would have been too high and the turbulent production would have been too low. We can obtain a balance between turbulent production and dissipation if we

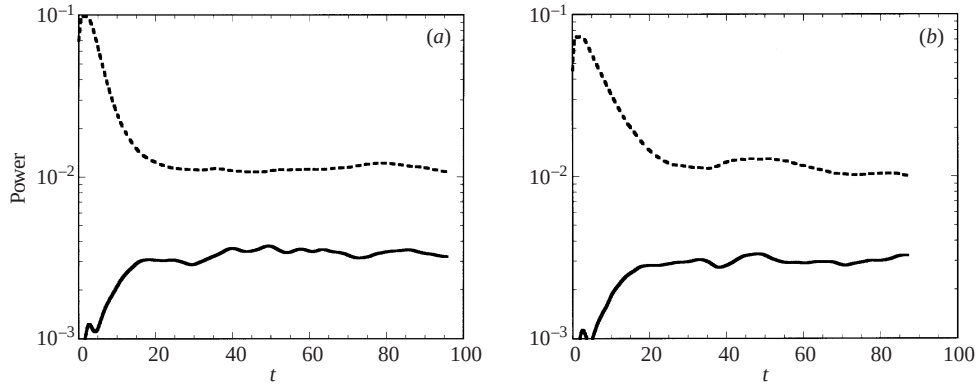

FIGURE 2. The adjustment period for the turbulent flow for neutrally stratified fluid, (*a*) $Re = 10^4$ and (*b*) $Re = 10^5$: ———, turbulent production rate and – – –, total dissipation rate. The power is normalized by U^3D^2.

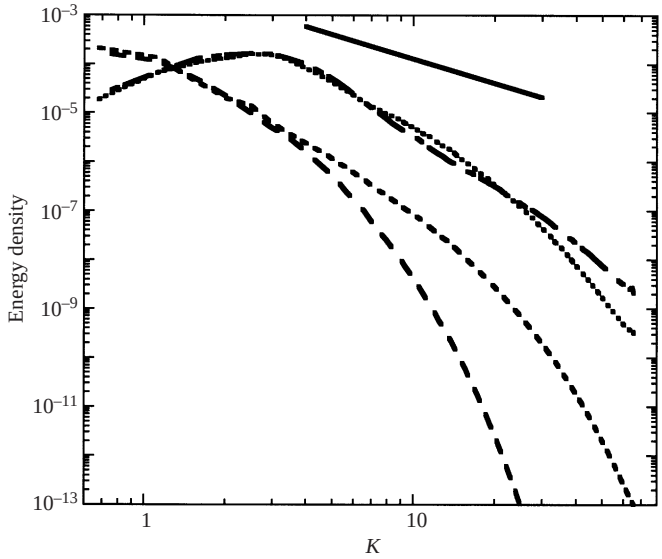

FIGURE 3. Initial and final turbulent kinetic energy spectra for neutrally stratified fluid: ·····, $Re = 10^4$, $t = 0$; – – –, $Re = 10^4$, $t = 902$; — · —, $Re = 10^5$, $t = 0$; - - - -, $Re = 10^5$, $t = 1007$; ———, $K^{-5/3}$. The spectral energy density is normalized by U^3D^4 and K is the wavenumber normalized by D^{-1}.

allow the normal Reynolds stresses to adjust. In this case, we found that the radial profiles for the r.m.s. fluctuating velocities became wider than was observed in the experiments.

Figure 3 shows the spectra of turbulent kinetic energy at the beginning (labelled $t = 0$ in the caption) and at the end of the simulations for $Re = 10^4$ and $Re = 10^5$, both for $Fr = \infty$. The spectra are normalized such that area beneath them equals the total turbulent kinetic energy integrated over the volume. For $Re = 10^5$, an extensive inertial range has been established. For $Re = 10^4$, the tail of the spectrum falls off more rapidly than for the high Reynolds number case, showing features of laminar flow.

The initial r.m.s. velocities and shear stress ($\langle \tilde{\tilde{u}}_1 \tilde{\tilde{u}}_r \rangle$), in which u_r is the radial com-

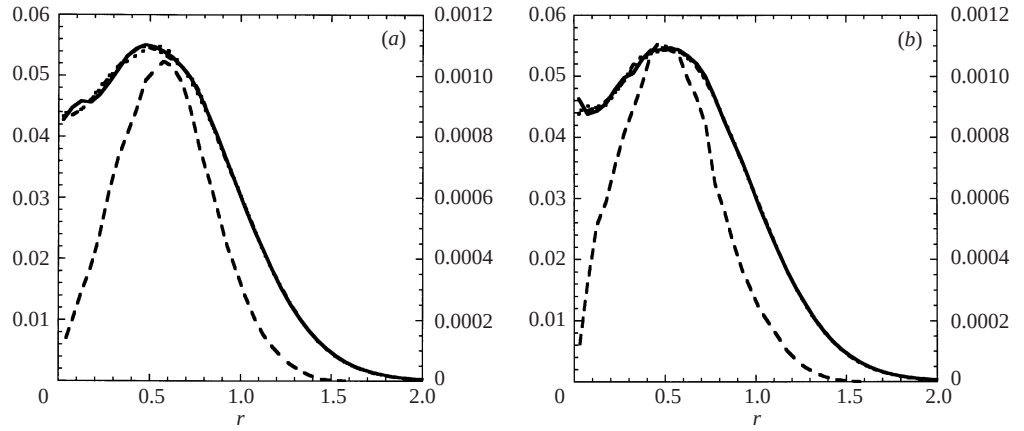

FIGURE 4. Initial conditions for (*a*) $Re = 10^4$ and (*b*) $Re = 10^5$: ———, $\langle\tilde{u}_1\tilde{u}_1\rangle^{1/2}$; — · —, $\langle\tilde{u}_2\tilde{u}_2\rangle^{1/2}$; · · · · · ·, $\langle\tilde{u}_3\tilde{u}_3\rangle^{1/2}$; – – –, $\langle\tilde{u}_1\tilde{u}_r\rangle$. r is the radial coordinate normalized by D. The scales for the r.m.s. velocities are on the left-hand axis of each plot, and the scales for the shear stress are on the right-hand axis.

ponent of velocity, are plotted in figure 4. Bevilaqua & Lykoudis (1978) report only the total of the r.m.s. velocities. We have assumed that the energy is equipartitioned among all three components and that all three components have the same axisymmetric radial distribution. Note that the r.m.s. velocity profiles have a peak off the axial axis and a local minimum at the axis. In the relaxation procedure, these profiles are held fixed while the shear stress is allowed to adjust. The final shear stress profile is shown in the figure to have a peak at the same location as the r.m.s. velocities. These profiles are similar to those that are reported in Uberoi & Freymuth (1970). Altogether, figures 3 and 4 provide enough information to duplicate the initial conditions for the cases that are reported here.

3.2. *Similarity*

As outlined briefly in the introduction, Spedding (1997) divides the evolution of a turbulent wake into three regimes that he identifies as the early (or near) wake, labelled $3D$ (for the three-dimensional, isotropic character of the wake and its turbulence), the intermediate wake, labelled NEQ (for the non-equilibrium period when potential energy is partially converted back to kinetic energy of the mean and turbulent flow), and the far (or late) wake, labelled $Q2D$ (for its quasi-two-dimensional characteristics). The duration of each of these regimes scales with N, which in our non-dimensionalization can be written in terms of the time $t^* = tFr^{-1}$. Spedding summarizes the existing laboratory studies for the towed-sphere wake and concludes that at time $t^*_I \approx 2$ the wake leaves the $3D$ regime and enters the NEQ regime and at time $t^*_{II} \approx 50$ the wake enters the $Q2D$ regime. Bonnier *et al.* (2000) insert a collapse regime, where the mean wake deficit actually increases with time, at the beginning of Spedding's NEQ. This collapse regime begins at $t^* \approx 2$ and ends at $t^* \approx 7$.

In the stratified simulations we present here, $Fr = 2$, so $t^* = 0.5t$. Our simulations are initiated with laboratory data from an $Fr = \infty$ experiment at $t^* = 3$, just at the beginning of the NEQ regime, in the collapse phase.

In a homogeneous fluid, the evolution of the mean and turbulent properties of the wake of a sphere are associated with various similarity laws which can be deduced from theory and have been verified by experiments. As reported in Spedding *et al.*

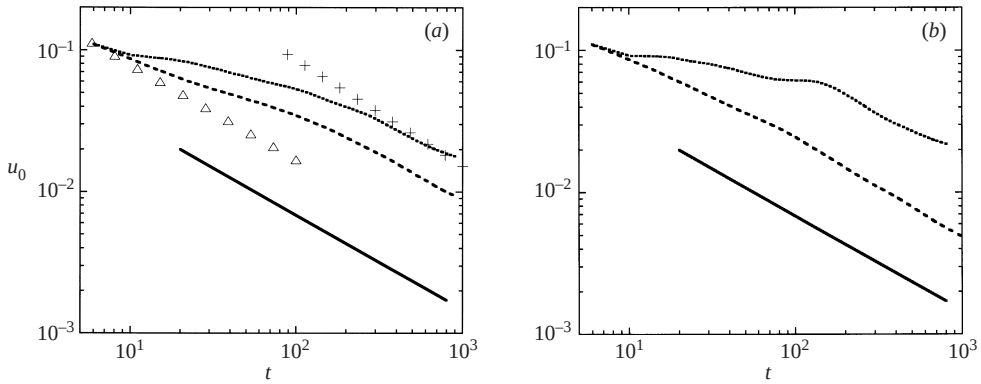

FIGURE 5. Centreline velocity deficit for $6 < t < 1000$ for (*a*) $Re = 10^4$ and (*b*) $Re = 10^5$: - - - -, $Fr = \infty$; △, $Fr = \infty$, fit to the data of Bevilaqua & Lykoudis (1978), figure 5*a*; ·····, $Fr = 2$; +, $Fr = 2$, fit to data of Spedding *et al.* (1996). The solid line represents $t^{-2/3}$.

(1996*a*, *b*) and Bonnier *et al.* (1998), laboratory measurements show that the mean and turbulent properties in the early and late wake of a sphere in a *stratified* fluid obey the same similarity laws as the wake in a *homogeneous* fluid, although the peak velocity deficit is up to an order of magnitude larger in the late wake of stratified flows. The physical quantities that we discuss here include the amplitude of the mean-wake deficit, the width and height of the wake, the mean and turbulent kinetic energy and the potential energy.

3.2.1. *Mean flow*

During the *NEQ* period, the vertical fluctuations radiate internal waves (Spedding 1997). As a result, the production term associated with $\tilde{\bar{u}}_1\tilde{\bar{u}}_3$ decreases more rapidly than the term associated with $\tilde{\bar{u}}_1\tilde{\bar{u}}_2$, and the wake spreads more rapidly in the horizontal plane than in the vertical plane. This effect can be quantified by fitting a Gaussian distribution of the following form to the mean velocity profile:

$$\langle \bar{u}_1 \rangle \approx u_o \exp\left(-\frac{1}{2}\left(\frac{x_2 - y_o}{r_y} \right)^2 - \frac{1}{2}\left(\frac{x_3 - z_o}{r_z} \right)^2 \right), \tag{3.2}$$

where u_o is the amplitude of the velocity deficit along the centreline, r_y is a measure of the width of the wake, and r_z is the corresponding height; y_o and z_o are respectively the centres of the wake along the x_2- and x_3-axes. The centres account for the meandering of the wake. A least-squares fit of the numerical data is used to fit the various coefficients.

Figures 5 and 6 respectively show the velocity amplitude and the length scales of the wake. For comparison, non-stratified fluid measurements of Bevilaqua & Lykoudis (1978) and the stratified fluid measurements of Spedding *et al.* (1996*b*), Bonnier *et al.* (1998) and Spedding (2002) are included for $Re = 10^4$. As shown in figure 5(*a*, *b*) the simulated u_o for $Fr = \infty$ initially follows the expected power-law behaviour ($t^{-2/3}$) and compares well with the laboratory results, but at $t \approx 10$ the simulations begin to deviate from the experimental results, decaying less rapidly, so that by $t \approx 100$ the simulated wake deficit is about twice that of the experiments. After $t \approx 100$ the simulated u_0 returns to a $t^{-2/3}$ behaviour, almost as if the simulated wake goes through an adjustment period. Curiously, the $Re = 10^5$ simulations produce a slightly better

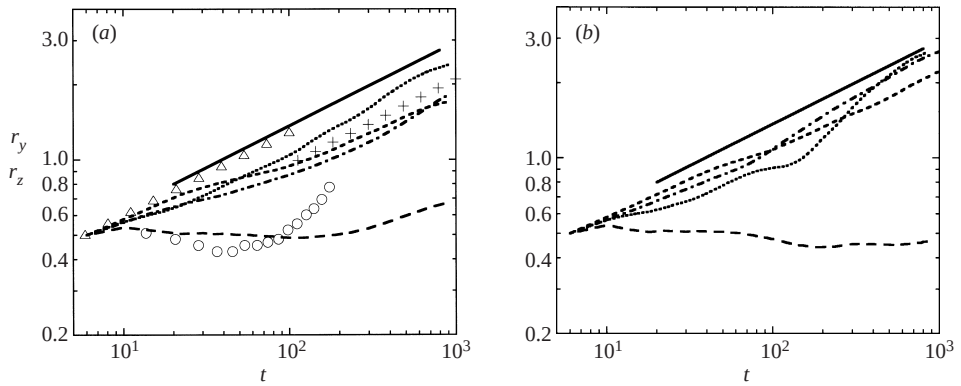

FIGURE 6. Wake width, r_y, and height, r_z, for $6 < t < 1000$ with (*a*) $Re = 10^4$ and (*b*) $Re = 10^5$: – – –, r_y for $Fr = \infty$; △, fit to $Fr = \infty$ data of Bevilaqua & Lykoudis (1978), figure 5*a*; · · · · · ·, r_y for $Fr = 2$; +, fit to r_y data of Bonnier *et al.* (1998), figure 4 and Spedding *et al.* (1996*b*), figure 10; — · —, r_z for $Fr = \infty$; — — —, r_z for $Fr = 2$; ○, r_z measured by Spedding (2002), figure 9*a*. The solid line represents $t^{1/3}$.

fit to the laboratory experiments. We attribute these discrepancies to the coefficients in the SGS model being too large, as noted previously.

When $Fr = 2$, the amplitude of the velocity deficit initially decays as in a non-stratified fluid, but starting at $t \approx 10$ it begins to decay less rapidly, which is evident in both the numerical and experimental results. At later times ($t \geqslant 120$), the numerical results for a stratified fluid show the same self-similar behaviour as a fluid that is not stratified. Furthermore, the initial onset of self-similarity is insensitive to Reynolds number. For $t \geqslant 120$ the simulated wake deficits are a very good match to the experimental measurements.

Figure 6(*a*, *b*) shows the horizontal, r_y, and vertical, r_z, length scales of the wake. When the fluid is not stratified laboratory experiments show that both length scales tend to grow like ($t^{1/3}$). In the simulations without stratification both length scales initially follow the $t^{1/3}$ behaviour. At the lower value of Re, as seen in figure 6(*a*), both length scales start to deviate from this behaviour at $t \approx 10$, increasing less rapidly than in the laboratory experiments. The simulations appear to return to the observed growth rates after $t \approx 100$, yet the wake width and height are substantially less than is observed in the experiments by this time. Again, as was found for the velocity deficit, the higher-Re simulations seem to be a better fit to the laboratory data.

In the simulations with stratification, the simulated wake initially spreads isotropically at the non-stratified rate, but at $t \approx 10$ the width of the wake begins to increase less rapidly and the height of the wake stops increasing, even slightly decreasing for a while. At $t \approx 30$ the width of the simulated wake begins to increase at a higher rate, matching the $t^{1/3}$ behaviour of the non-stratified wake, and surpassing the simulated non-stratified wake width at $t \approx 50$. The height of the simulated wake stays fairly constant until $t \approx 120$, when it starts to increase slowly. The agreement with laboratory data for the stratified case is quite good for r_y in the late wake and reasonably good for r_z in the intermediate wake, but the laboratory measurements show the wake height starting to increase sooner and at a substantially faster rate than in the simulations. Comparing figures 6(*a*) and 6(*b*), it can be seen that the growth of the wake in a stratified fluid changes somewhat with Reynolds number. In particular, the vertical spreading of the wake is less and the horizontal spreading slightly greater for the higher Reynolds number.

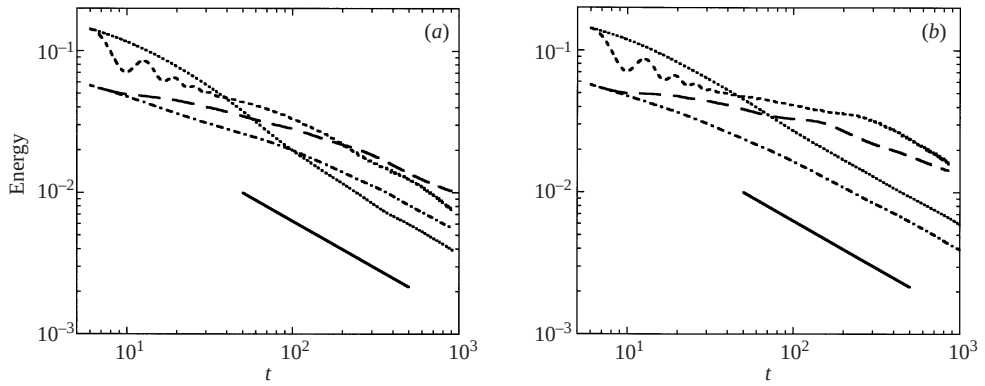

FIGURE 7. Kinetic energy for $6 < t < 1000$ for (*a*) $Re = 10^4$ and (*b*) $Re = 10^5$: ·····, fluctuations for $Fr = \infty$; — · —, mean flow for $Fr = \infty$; - - - -, fluctuations for $Fr = 2$; — — —, mean flow for $Fr = 2$. The solid line represents $t^{-2/3}$. The energy is normalized by U^2D^3.

3.2.2. *Energetics*

Based on laboratory measurements of the wakes of spheres in non-stratified fluids, volume integrals of both the mean and of the turbulent kinetic energy decay approximately as $t^{-2/3}$, which is consistent with the mean and r.m.s. velocities decaying as $t^{-2/3}$ and both the horizontal and vertical length scales of the wake increasing as $t^{1/3}$. Spedding *et al.* (1996*a*, *b*) found the same self-similar behaviour for wakes of spheres in stratified fluids sufficiently far downstream.

In figure 7 the kinetic energy in the mean portion of the flow integrated over the volume of fluid ($\int_{\mathscr{V}} \mathrm{d}V\langle\bar{u}_i\rangle\langle\bar{u}_i\rangle$) and the turbulent kinetic energy ($\int_{\mathscr{V}} \mathrm{d}V\tilde{\bar{u}}_i\tilde{\bar{u}}_i$) are plotted versus time for both the non-stratified and stratified cases for (*a*) $Re = 10^4$ and (*b*) $Re = 10^5$. The energy in the mean flow for the non-stratified cases decays from the beginning as $t^{-2/3}$, as expected. The turbulent kinetic energy for $Re = 10^5$ with no stratification is also self-similar for $t \geqslant 30$. This is consistent with Bevilaqua & Lykoudis (1978) who had observed that turbulence quantities tend to take longer than mean-flow quantities to reach self-similarity.

The energy in the mean flow for the stratified cases shows a self-similar behaviour for $t \geqslant 120$, decaying as $t^{-2/3}$ for $Re = 10^4$, but slightly more slowly for $Re = 10^5$. The lower Reynolds number result is consistent with Spedding *et al.*'s (1996*a*, *b*) experimental observations. Also, as noted by Spedding *et al.* (1996*a*) and confirmed by the present numerical results, the duration of the non-equilibrium period for the mean flow seems to be insensitive to Reynolds number. For the stratified fluids, the oscillations in the turbulent kinetic energy are associated with the generation of internal waves. During the initial stages, the vertical fluctuations in velocity radiate internal waves. There is a decrease in the vertical component of kinetic energy and a corresponding increase in the potential energy associated with the generation of internal waves. Note that the LES is initialized such that the internal wave field is not in adjustment, which may also contribute to this effect.

For each Reynolds number, the turbulent kinetic energy initially decreases by more for the stratified fluid than the non-stratified fluid. Conversely, the mean-flow kinetic energy initially increases by more for the stratified fluid than the non-stratified fluid. As internal waves are radiated, the turbulent production term associated with $\tilde{\bar{u}}_1\tilde{\bar{u}}_3$ decreases more rapidly than it would in a non-stratified fluid because the vertical fluctuations $\tilde{\bar{u}}_3$ are reduced as a result of the radiation of internal waves. The turbulent

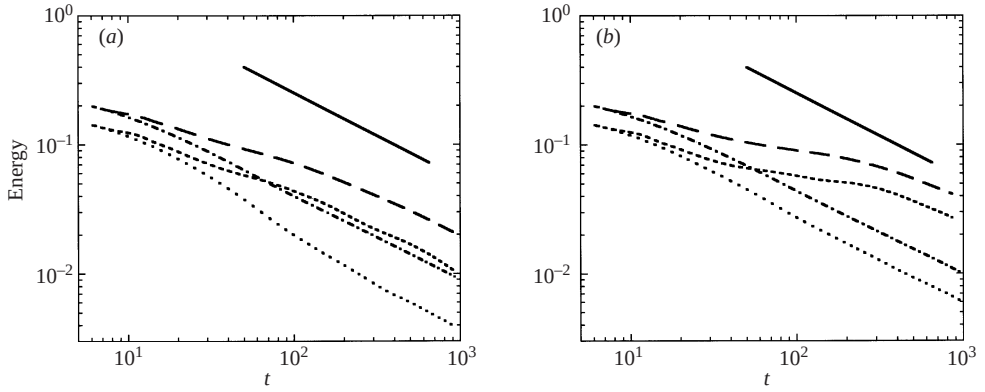

FIGURE 8. Total potential and kinetic energies for $6 < t < 1000$ for (*a*) $Re = 10^4$ and (*b*) $Re = 10^5$. The results for non-stratified fluids ($Fr = \infty$) are: ·····, turbulent kinetic energy $\tilde{E}$; — · —, total energy (E). The results for stratified fluids ($Fr = 2$) are: - - - -, turbulent kinetic energy plus potential energy $\tilde{E}$; — — —, total energy (E). The solid line represents $t^{-2/3}$. The energy is normalized by U^2D^3.

production is reduced and less energy is drained from the mean flow into turbulence. A similar effect is observed by Sarkar (2000) in his numerical simulations of turbulent shear flows in a stratified fluid.

As noted by Spedding (1997), energy is redistributed between the kinetic energy and the potential energy and also between the mean and the fluctuating portions of the flow. Figure 8 shows the total energy (E), which includes the turbulent kinetic energy, the kinetic energy in the mean portion of the flow, and the *turbulent potential energy* $((1/Fr^2)\int_0^t \mathrm{d}\tau \int_{\mathscr{V}} \mathrm{d}V \tilde{\rho}\tilde{u}_3)$. The potential energy in the mean portion of the flow is two orders of magnitude less than the potential energy due to fluctuating quantities. Figure 8 also shows the total energy in the fluctuating portion of the flow ($\tilde{E}$), which includes the turbulent kinetic energy and the turbulent potential energy. The stratified and non-stratified fluids establish self-similarity for both E and $\tilde{E}$. The results for both Reynolds numbers show a tendency in the far wake for the energy in the stratified fluid to be higher than in the non-stratified fluid. This effect may be attributed to the generation of compact and energetic vortex structures in the stratified late wake as well as the presence of internal waves.

Figure 9(a, b) shows how the energy in the fluctuating portion of the flow is distributed between kinetic and potential energies. The vertical component of turbulent kinetic energy ($\int_{\mathscr{V}} \mathrm{d}V \tilde{u}_3\tilde{u}_3$) is dominated by the radiation of internal waves, which also manifests itself in the plot of potential energy. Note that the potential energy is initially zero because of the way the initial conditions are prescribed. Aside from a slight difference in the decay rate, the magnitude and phase of the radiated energy are not sensitive to either the Reynolds number or the initial phase of the velocity field. The oscillations in the kinetic and potential energies occur at twice the normalized buoyancy frequency, where the normalized buoyancy frequency is Fr^{-1}. The period of the oscillations is $T = \pi F_r$. Riley, Metcalfe & Weissman (1981) observe a similar effect in their direct numerical simulations of homogeneous turbulence in stratified fluids.

Except for an initial dip, the horizontal component of the turbulent kinetic energy ($\int_{\mathscr{V}} \mathrm{d}V(\tilde{\tilde{u}}_1\tilde{\tilde{u}}_1 + \tilde{\tilde{u}}_2\tilde{\tilde{u}}_2)$) is not influenced by the generation of internal waves. As shown in figure 9, there is a corresponding initial rise in the sum of the vertical component

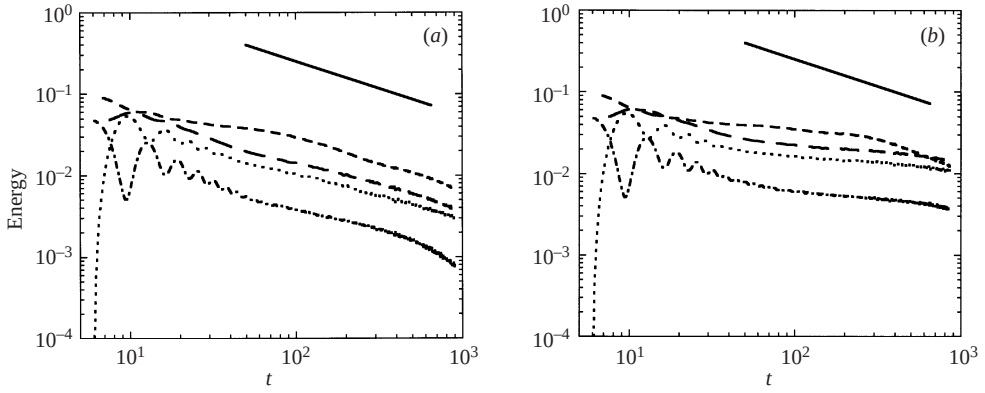

FIGURE 9. Distribution of energy in the fluctuating portion of the flow for $6 < t < 1000$ for (a) $Re = 10^4$ and (b) $Re = 10^5$. The curves are labelled as follows: — · —, vertical component of turbulent kinetic energy; ·····, turbulent potential energy; — — —, vertical component of turbulent kinetic energy plus turbulent potential energy; - - - -, horizontal component of turbulent kinetic energy. The solid line represents $t^{-2/3}$. The energy is normalized by U^2D^3.

of turbulent kinetic energy plus potential energy. In the NEQ regime ($10 < t < 120$) the vertical component of the turbulent kinetic energy decays more rapidly than the horizontal component, but later in the Q2D regime the two components decay at a comparable rate, which has also been observed by Sarkar (2000). This effect may be attributed to the coupling that exists among the velocity components through the pressure gradient term in the momentum equations.

3.3. *The formation of pancake eddies*

Figures 10 and 11 show time series of the vertical component of vorticity in the horizontal plane through the wake centreline ($x_3 = 0$) for respectively $Re = 10^4$ and $Re = 10^5$. Part (a) of each figure illustrates the results for the non-stratified fluid ($Fr = \infty$), and part (b) shows the corresponding results for a stratified fluid ($Fr = 2$). In this grey-scale figure, white represents positive vorticity with magnitude $\omega_z = 4$ and black negative vorticity with $\omega_z = -4$. Each frame has the dimensions $24D$ in both the cross-stream and upstream (to the right) directions. Note that the flow along the streamwise direction (x_1) has been periodically extended one additional computational domain length. The centres of each frame are located at (from left to right and top to bottom) $t \approx 6$, 14, 30, 46, 62, 86, 134, 166, 198, 262, 326, 390, 454, 550, 678 and 838. The vorticity in each frame is scaled by the distance downstream, which is the expected similarity behaviour.

Comparing figure 10(a) with figure 11(a) shows that the higher-Reynolds-number case has finer structure than the lower-Reynolds-number case. For the stratified cases, coherent structures, in the form of nearly circular vortex patches, begin to appear at $t \approx 100$. This corresponds to the end of the NEQ regime, when the mean kinetic energy begins to decay at the late-wake self-similar rate. Note that instabilities are evident almost immediately. Further downstream, the size of these patches of vorticity grows and the number of patches in a frame very slowly decreases. For $Re = 10^4$, there are roughly four vortex pairs in each frame for $t \geqslant 200$. The number and shape of the vortex pairs compares well with the experimental results of Spedding *et al.* (1996*a*).

To describe the formation of the pancake eddies Spedding *et al.* (1996*a*) define a Strouhal number $St \equiv D/\lambda_x$ based on the spacing in the axial direction between

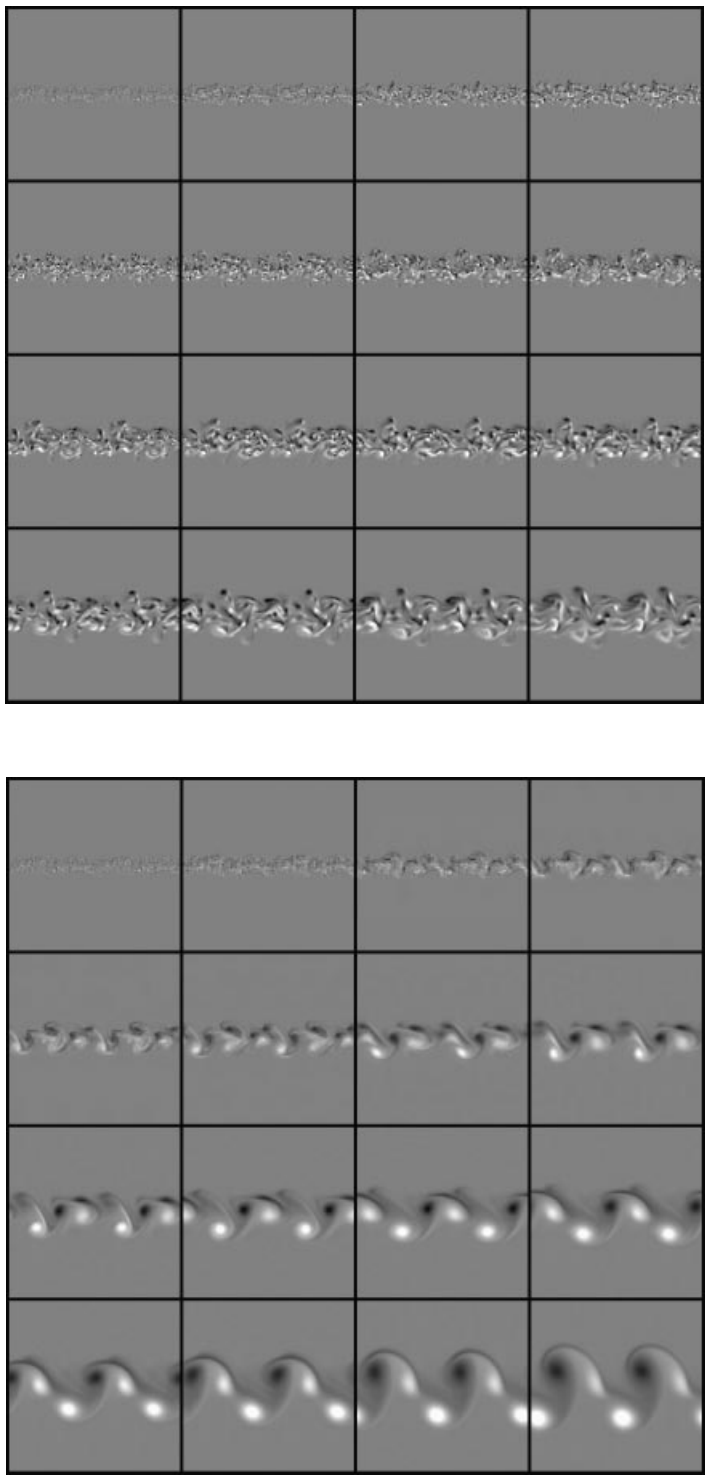

FIGURE 10. A time history of the vertical component of vorticity ω_z on the horizontal plane ($x_3 = 0$) through the centre of the wake, for the case with $Re = 10^4$: (*a*) $Fr = \infty$ and (*b*) $Fr = 2$. The images are at the times, from left to right, top to bottom: $t \approx 6$, 14, 30, 46, 62, 86, 134, 166, 198, 262, 326, 390, 454, 550, 678 and 838.

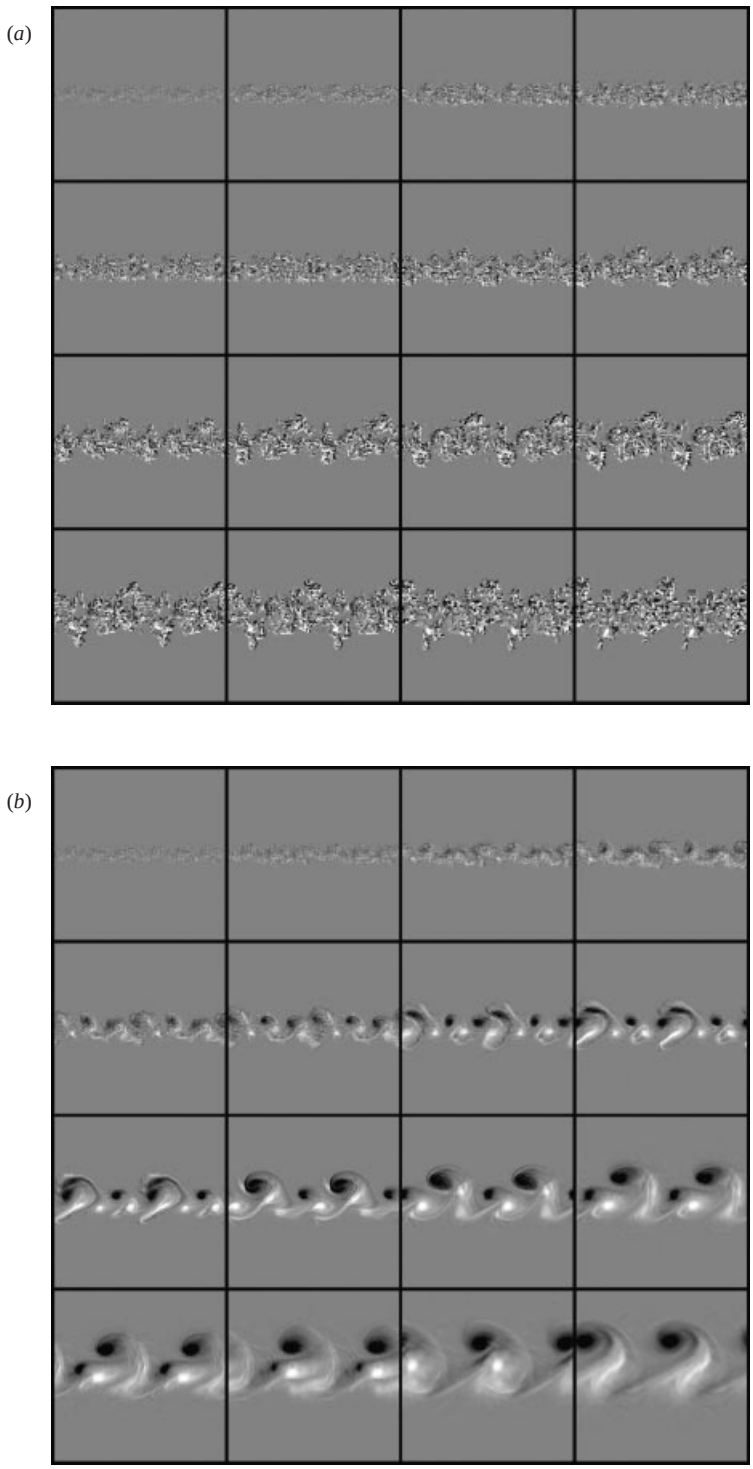

FIGURE 11. A time history of the vertical component of vorticity ω_z on the horizontal plane ($x_3 = 0$) through the centre of the wake, for the case with $Re = 10^5$: (*a*) $Fr = \infty$ and (*b*) $Fr = 2$. The images are at the times, from left to right, top to bottom: $t \approx 6$, 14, 30, 46, 62, 86, 134, 166, 198, 262, 326, 390, 454, 550, 678 and 838.

the vortex cores, λ_x. For $Fr = 2$, Spedding *et al.* (1996*a*) measure a Strouhal number $St \approx 0.173$ in the range $50 \leqslant t \leqslant 125$. The wavelength that is associated with this Strouhal number roughly corresponds to four vortex pairs per frame in figure 10(*b*), which is observed when $t \geqslant 200$. We conjecture that large-scale pancake eddies are established earlier in Spedding *et al.*'s (1996*a*) laboratory experiments because our numerical simulations are initialized using a wake relaxation procedure that is used to establish self-similarity. As a result, the initial spectrum of our numerical simulation is probably more broad than the laboratory measurements. This speculation is supported by comparing Spedding *et al.*'s (1996*a*) figure 3 to our figure 10(*b*), which shows that finer structures are initially present in the numerical simulations that are not visible in the laboratory experiments. Spiral-vortex instabilities appear to promote the formation of large pancake eddies in the near wake, but the results of our numerical simulations indicate that spiral-vortex instabilities are not necessary to form pancake eddies. In fact, our numerical simulations indicate that pancake eddies appear to form over a very broad range of wavenumbers. These numerical results are important because they illustrate that pancake eddies can form without the flow being 'seeded' with some initial structure. In the experimental results of Spedding *et al.* (1996*a*, *b*), Spedding (1997), and Chomaz *et al.* (1993*a*) the late wake preserves some information about structures in near wake, such as the structure of the helical instability mode. We conclude from a comparison of the numerical simulations and the experiments that any structures present in the near wake can have some affect on the far-wake structure, but that they are not essential for the formation of far-wake eddies. This conclusion is consistent with the conclusions described in Bonnier *et al.* (1998, 2000) based on experiments using both laminar and turbulent wakes.

For $Re = 10^5$, vortex merging is more pervasive and as a result there are fewer vortex pairs evident in the stratified-flow simulation than are present at the lower Reynolds number. For the non-stratified fluid (see figure 11*a*), there are two bulges in the contours of the vorticity. (Note that there is really only one bulge in the computational domain because the data in the figures have been periodically extended.) These bulges may have contributed to the dissimilar behaviour that is observed in the mean velocity profiles that are plotted in figures 5(*b*) and 6(*b*). The positions of the bulges in the non-stratified results (see figure 11*a*) and the positions of the largest pancake eddies in the stratified results (see figure 11*b*) roughly correspond. Over the duration of the simulation, the small-scale features that are observed in the bulges of the non-stratified simulation appear to merge to form the large-scale structures that are observed toward the end of the stratified simulation.

4. Conclusions

We have presented some preliminary results from using an LES scheme to compute the late wake of a sphere towed at constant speed through a non-stratified and a uniformly stratified fluid. For each case, we have obtained results corresponding to two Reynolds numbers, one representative of laboratory scale and the other much higher.

An important aspect of the simulations is the use of a relaxation procedure to adjust the initial turbulence fields so that the normal and shear turbulent stresses are properly correlated and the turbulent production and dissipation are in equilibrium. Using this relaxation procedure to determine the proper turbulent initial conditions produces wakes with similarity behaviour that matches what is observed in the experiments. This ability to match the similarity behaviour of the experiments is a

good indication that the subgrid-scale model in this LES scheme is suitably modelling the subgrid-scale turbulence.

The numerical study of Gourlay *et al.* (2001) involves a spectral DNS of a drag wake with $Re = 10^4$ and $Fr = 5$ and ∞, and focuses on the far-field properties of the wake. As in the present study, they use a Galilean approximation to relate the spatial evolution of the wake to the temporal evolution of the flow in the simulation domain. The turbulent field is initialized using random phases, and contrary to the present study, a relaxation procedure is not used to establish the turbulent shear stresses and bring the initial turbulent production and dissipation into equilibrium. Nevertheless, Gourlay *et al.*'s (2001) results for the properties of the far-field wake are similar to those obtained in the present study. We have found that achieving the appropriate initial turbulence properties of the wake is essential for accurately simulating the near- to intermediate-field wake, but is not important if only the far-field wake is of interest.

We have found in the stratified case, consistent with the conclusions from previous laboratory and numerical studies, that the wake flow does not need to be 'seeded' with some coherent structure in order to develop well-ordered 'pancake eddies' in the far field, although the near-field wake structure may play a role in how the flow evolves towards its late-wake structure. This is true for both Reynolds numbers. In fact, most aspects of the wake appear to be insensitive to the Reynolds number. In general the wake has finer structure at the higher Reynolds number, and evolves differently than it does at lower Reynolds number, but the far-field result is similar.

This research is supported by ONR under contract number N00014-01-C-0191, Dr L. Patrick Purtell program manager. This work was supported in part by a grant of computer time from the DOD High Performance Computing Modernization Program at the Naval Oceanographic Office Major Shared Resource Center. We thank Professor G. R. Spedding at the University of Southern California for sharing his laboratory data with us and for many helpful discussions. We thank the reviewers for their very thorough and helpful reviews.

REFERENCES

Bardina, J., Ferziger, J. H. & Reynolds, W. C. 1984 Improved turbulence models based on LES of homogeneous incompressible turbulent flows. *Rep. TF-19*. Dept. of Mechanical Engineering, Stanford University.

Bevilaqua, P. M. & Lykoudis, P. S. 1978 Turbulence memory in self-preserving wakes. *J. Fluid Mech.* **89**, 589–606.

Bonnier, M., Bonneton, P. & Eiff, O. 1998 Far-wake of a sphere in a stably stratified fluid: characterization of the vortex structures. *Appl. Sci. Res.* **59**, 269–281.

Bonnier, M., Eiff, O. & Bonneton, P. 2000 On the density structure of far-wake vortices in a stratified fluid. *Dyn. Atmos. Oceans* **31**, 117–137.

Chomaz, J.-M., Bonneton, P., Butet, A. & Hopfinger, E. J. 1993*a* Vertical diffusion of the far wake of a sphere moving in a stratified fluid. *Phys. Fluids* A **5**, 2799–2806.

Chomaz, J.-M., Bonneton, P., Butet, A., Perrier, M. & Hopfinger, E. J. 1992 Froude number dependence of the flow separation line on a sphere towed in a stratified fluid. *Phys. Fluids* A **4**, 254–258.

Chomaz, J. M., Bonneton, P. & Hopfinger, E. J. 1993*b* The structure of the near wake of a sphere moving horizontally in a stratified fluid. *J. Fluid Mech.* **254**, 1–21.

Dommermuth, D. G., Gharib, M., Huang, H., Innis, G. E., Maheo, P., Novikov, E., Talcott, J. C. & Wyatt, D. C. 1997 Turbulent free-surface flows: a comparison between numerical simulations and experimental measurements. In *Proc. Twenty-first Symp. on Naval Hydrodynamics, Trondheim*, pp. 249–265. National Academy Press.

Dommermuth, D. G., Rottman, J. W., Innis, G. E. & Novikov, E. 2000 Numerical simulation of the wake of a towed sphere in a weakly stratified fluid. In *Stratified Flows I: Proc. 5th Intl Symp. on Stratified Flows, Vancouver, Canada* (ed. G. A. Lawrence, R. Pieters & N. Yonemitsu), pp. 37–42. University of British Columbia.

Fung, Y. T. & Chang, S. W. 1996 Surface and internal signatures of organized vortex motions in stratified fluids. *Phys. Fluids* **8**, 3023–3056.

Germano, M., Piomelli, U., Moin, P. & Cabot, W. H. 1991 A dynamic subgrid-scale eddy viscosity model. *Phys. Fluids* A **3**, 1760–1765.

Gilreath, H. E. & Brandt, A. 1985 Experiments on the generation of internal waves in a stratified fluid. *AIAA J.* **23**, 693–700.

Gourlay, M. J., Arendt, S. C., Fritts, D. C. & Werne, J. 2001 Numerical modeling of initially turbulent wakes with net momentum. *Phys. Fluids* **13**, 3783–3802.

Hopfinger, E. J. 1987 Turbulence in stratified fluids: a review. *J. Geophys. Res.* **C92**, 5287–5303.

Kao, T. W. & Pao, H. P. 1978 Note on the flow of a stratified fluid over a stationary obstacle in a channel. *Geophys. Astrophys. Fluid Dyn.* **10**, 109–114.

Lin, J. T. & Pao, Y. H. 1979 Wakes in stratified fluids: a review. *Annu. Rev. Fluid Mech.* **11**, 317–338.

Lin, Q., Boyer, D. L. & Fernando, H. J. S. 1992*a* Turbulent wakes of linear stratified flow past a sphere. *Phys. Fluids* A **4**, 1687–1696.

Lin, Q., Boyer, D. L. & Fernando, H. J. S. 1994 The vortex shedding of a streamwise-oscillating sphere translating through a linearly stratified fluid. *Phys. Fluids* **6**, 239–252.

Lin, Q., Lindberg, W. R., Boyer, D. L. & Fernando, H. J. S. 1992*b* Stratified flow past a sphere. *J. Fluid Mech.* **240**, 315–354.

Orszag, S. A. & Pao, Y. H. 1974 Numerical computation of turbulent shear flows. In *Proc. Symp. Turbulent Diffusion in Environmental Pollution* (ed. F. N. Frenkiel & R. E. Mann), pp. 225–236. Academic.

Pao, H. P. & Kao, T. W. 1977 Vortex structure in the wake of a sphere. *Phys. Fluids* **20**, 187–191.

Riley, J. J. & Lelong, M.-P. 2000 Fluid motions in the presence of strong stable stratification. *Annu. Rev. Fluid Mech.* **32**, 613–657.

Riley, J. J., Metcalfe, R. W. & Weissman, M. A. 1981 Direct numerical simulations of homogeneous turbulence in density stratified fluids. In *Nonlinear Properties of Internal Waves* (ed. B. J. West), pp. 79–112. Am. Inst. Physics.

Sarkar, S. 2000 Turbulence anisotropy in stratified uniform shear flow. In *Proc. Fifth Intl Symp. on Stratified Flows, Vancouver* (ed. G. A. Lawrence, R. Pieters & N. Yonemitsu), pp. 1245–1250. University of British Columbia.

Schooley, A. & Stewart, R. W. 1963 Experiments with a self-propelled body submerged in a fluid with a vertical density gradient. *J. Fluid Mech.* **15**, 83–96.

Spedding, G. R. 1997 The evolution of initially turbulent bluff-body wakes at high internal Froude number. *J. Fluid Mech.* **337**, 283–301.

Spedding, G. R. 2001 Anisotropy in turbulence profiles of stratified wakes. *Phys. Fluids* **13**, 2361–2372.

Spedding, G. R. 2002 Vertical structure in stratified wakes with high initial Froude number. *J. Fluid Mech.* **454**, 71–112.

Spedding, G. R., Browand, F. K. & Fincham, A. M. 1996*a* The long-time evolution of the initially turbulent wake of a sphere in a stable stratification. *Dyn. Atmos. Oceans* **23**, 171–182.

Spedding, G. R., Browand, F. K. & Fincham, A. M. 1996*b* Turbulence, similarity scaling and vortex geometry in the wake of a towed sphere in a stably stratified fluid. *J. Fluid Mech.* **314**, 53–103.

Staquet, C. & Godeferd, F. S. 1998 Statistical modelling and direct numerical simulations of decaying stably stratified turbulence. Part 1. Flow energetics. *J. Fluid Mech.* **360**, 295–340.

Sysoeva, E. Ya. & Chashechkin, Yu. D. 1991 Vortex systems in the stratified wake of a sphere. *Fluid Dyn.* **26**, 544–551.

Uberoi, M. S. & Freymuth, P. 1970 Turbulent energy balance and spectra of the axisymmetric wake. *Phys. Fluids* **13**, 2205–2210.